Tribology Letters (2023) 71:57
https://doi.org/10.1007/s11249-023-01728-1

ORIGINAL PAPER

Possible Origin of D- and G-band Features in Raman Spectra of Tribofilms

Yu-Sheng Li[1] · Seokhoon Jang[1] · Arman Mohammad Khan[2] · Tobias V. Martin[2] · Andrew L. Ogrinc[1] · Q. Jane Wang[2] · Ashlie Martini[3] · Yip-Wah Chung[2,4] · Seong H. Kim[1]

Received: 11 January 2023 / Accepted: 27 March 2023

Abstract
In the Raman analysis of tribofilms produced from organic precursors, the D- and G-band features are often observed, which resemble the characteristic bands of diamond-like carbon (DLC), amorphous carbon (a-C), or graphitic materials. This study reports experimental evidence that the D- and G-bands features in the Raman spectra of tribofilms could be generated by photochemical degradation of triboproducts due to the focused irradiation of laser beam during the Raman analysis, indicating that they are not unique to the genuine structure of the tribofilm produced via friction. This finding suggests that other complementary and non-destructive characterization is required to determine whether DLC, a-C, or graphitic species are produced tribochemically by frictional shear.

Graphical Abstract

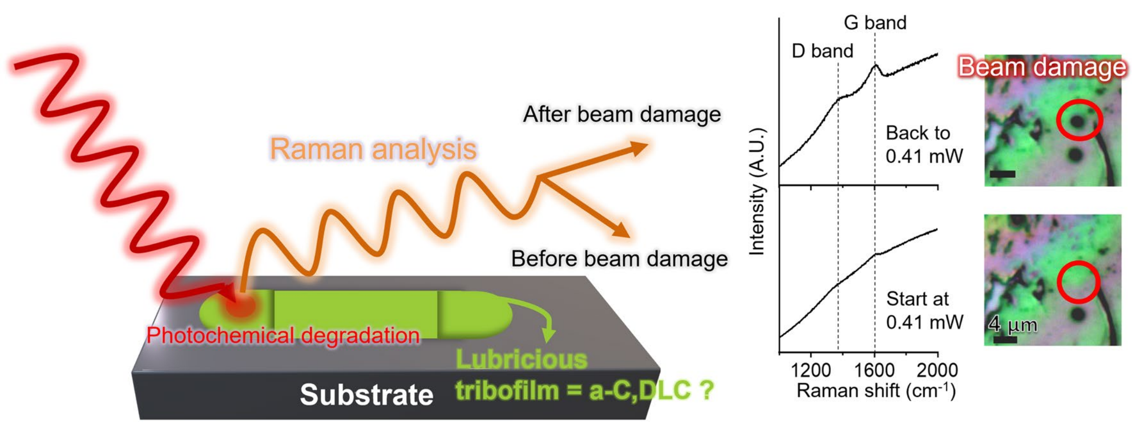

Keywords Tribochemistry · Diamond-like carbon · Laser damage · Photochemical degradation

✉ Yip-Wah Chung
ywchung@northwestern.edu

✉ Seong H. Kim
shk10@psu.edu

1 Department of Chemical Engineering and Materials Research Institute, Pennsylvania State University, University Park, PA 16802, USA

2 Department of Mechanical Engineering, Northwestern University, Evanston, IL 60208, USA

3 Department of Mechanical Engineering, University of California, Merced, CA 95343, USA

4 Department of Materials Science and Engineering, Northwestern University, Evanston, IL 60208, USA

Published online: 15 April 2023

1 Introduction

Organic molecules can undergo various chemical reactions at sliding interfaces [1]. Such reactions are specifically called tribochemical reactions and can be driven thermally via frictional heat or mechanochemically via shear-induced activation [2-4]. The resulting surface layers formed through tribochemical reactions are called tribofilms and can provide beneficial lubrication properties [5-10]. Tribofilms, present inside the sliding track or piled up around the contact region, are often analyzed by Raman spectroscopy [11-38]. This technique is widely used because it provides vibrational spectroscopic information from small amounts of samples. When the excitation beam is focused onto a small area through an optical microscope (as in confocal Raman spectroscopy), the sample within a 1 ~ 10 μm^2 area can be analyzed with good detection efficiency of the scattered Raman signal [39, 40]. Thus, Raman spectroscopy is well suited for the analysis of tribofilms that are accumulated in a small area.

Many Raman spectra of tribofilms reported in the literature showed two vibrational bands at ~ 1360 cm^{-1} and ~ 1570 cm^{-1} [11-38, 41, 42]. Numerous examples found in the literature are organized in Table S1 in the Supporting Information, in which readers can see that the types of tribofilms and Raman analysis conditions vary drastically. The spectral features at ~ 1360 cm^{-1} and ~ 1570 cm^{-1} resemble the characteristic peaks, called the D- and G-bands, respectively, of diamond-like carbon (DLC), amorphous carbon (a-C), or graphitic materials [11, 14-27, 29-38]. DLC and a-C are known to be good solid lubricant materials with excellent lubricating efficiency and superior wear resistance [43-49]. Thus, if such materials were produced by frictional shear via tribochemical reactions, that would be very beneficial for lubrication purposes.

However, it is noted that most DLC and a-C films with good lubrication properties are produced by high-energy processes such as physical vapor deposition (PVD) via magnetron sputtering or plasma-enhanced chemical vapor deposition (PECVD) [43, 45, 50]. Various types of a-C can be produced via pyrolysis of organic precursors, but it requires quite high temperatures (> 700–800 °C) and often oxygen-lean conditions [51-55]. Frictional heat generated during the sliding process in most tribo-testing conditions is not high enough to induce carbonization of organic products or residues. Representative calculations of flash temperature rise due to frictional heat are given in the Supporting Information. In many studies, DLC-like or a-C tribofilms were presumed to form via tribochemical reactions of organic precursors at flash temperatures far lower than typical temperatures required for thermal decomposition or pyrolysis of organic compounds. Such conclusions were primarily drawn based on the observation of the D- and G-band features in Raman analysis of tribofilms [16, 21, 33]. This leads to the following question: Are the D- and G-band features in Raman spectra of tribofilms sufficient to confirm that tribofilms contain DLC, a-C, or even graphitic material?

Reported in this paper is experimental evidence indicating that the D- and G-band features in Raman spectra of tribofilms may originate from *post-synthesis* photochemical degradation of carbonaceous organic matters during the Raman analysis. This finding suggests that the observation of the D- and G-band features in Raman spectra is not sufficient to say that DLC, a-C, or graphitic species are produced via tribochemical reactions assisted by interfacial friction or shear of organic molecules. Therefore, other complementary characterization methods [37, 56] are necessary to test the hypothesis of producing DLC, a-C, or graphitic species by friction.

1.1 Experimental Details

Vapor phase lubrication (VPL) conditions were first used to produce tribofilms on two different substrates, AISI 440C stainless steel (SS; McMaster-Carr) and 4 mm thick soda lime silicate (SLS; PPG) glass. The SS plate was polished with sandpaper and alumina slurry to the root-mean-square surface roughness (R_q) of ~ 20 nm. Note that high-vapor-pressure products of tribochemical reactions were lost into the gas phase and only the tribofilms remaining in or around the sliding track were analyzed [57, 58]. The precursor was methylcyclopentane and its partial pressure was about 3750 Pa at 20 °C (30% with respect to its saturation vapor pressure) [28]. The saturated vapor of methylcyclopentane was generated by flowing dry N_2 (moisture volume concentration ~ 18 ppm) through a flask filled with methylcyclopentane liquid. An AISI 440C stainless steel ball (diameter = 3 cm; $R_q \approx 6$ nm [9]) was placed and loaded with a 0.5 N force against the SS plate. At this load, the maximum Hertzian contact pressure was estimated to be 450 MPa. A borosilicate glass ball (Pyrex; diameter = 3 mm) was used as the counter-body to the glass plate at a normal load (0.5 N) that generated the maximum Hertzian contact pressure of 320 MPa. For both material systems, the sliding speed was 3 mm/s and the total sliding time was 18 min. With these experimental conditions, the flash temperature due to frictional heat was calculated to be 0.5 °C on the SS plate [59] (see the Supporting Information for calculation details). The produced tribofilms were analyzed with Raman spectroscopy using a Horiba LabRam HR Evolution Vis–NIR system. The excitation wavelengths were 532 nm, 633 nm, and 785 nm, and the excitation laser was focused with an objective lens 50 × (NA = 0.5) or 100 × (NA = 0.9). The exposure time was 1 s and 10 accumulations. The thickness of the tribofilms was measured with atomic force microscopy (AFM; Bruker Digital Instrument Multimode).

Oil-lubricated conditions were also tested, which were more relevant to industrial conditions. A multi-functional tribometer (RTEC MFT-5000) with a reciprocating module was used to produce the tribofilm deposit on the ball. The flat AISI 52100 steel samples were heat-treated to obtain Vickers hardness of 311 ± 22 HV. The heat treatment procedure consisted of austenization treatment at 900 °C for 1 h in air, followed by quenching in water at room temperature and then aging at 550 °C for 1 h. The flat samples were then polished using the standard metallographic technique to an average R_q of ~ 22 nm. An AISI 52100 steel ball (52100 ball) with a diameter of 9.5 mm and R_q of ~ 5.6 nm was used. Tribological tests were conducted at 25 °C and about 24% relative humidity under a normal load of 2 N, a reciprocating frequency of 5 Hz, and a stroke length of 10 mm, using PAO-4 as the lubricant. This normal load corresponded to a maximum Hertzian contact pressure of 611 MPa. After 1 h of tribo-testing, a dark-colored deposit was accumulated on the ball, which was then rinsed with hexane to remove the residual lubricant. Raman spectra were collected using a Horiba LabRam HR Evolution confocal Raman microscope with the excitation laser wavelength of 473 nm and a 100 × objective lens (NA = 0.95) to select the region of interest for the analysis. The laser power used for data collection varied between 1 to 10% of the full power (25 mW). The exposure time was 30 s and 3 accumulations.

A further study of the tribofilms generated in oil-lubricated conditions was conducted at a faster speed and run for longer time using a different lubricant, dodecane, subjected to boundary lubrication conditions. This experiment was performed with a flat D2 steel sample and a 52100 ball. Both substrate and ball have a Vickers hardness of about 800 HV. The flat D2 substrate was used for this experiment instead of 52100 because a larger production of tribofilm was observed with the D2 steel than 52100 when lubricated with dodecane [29]. The test was conducted for 5 h at normal load of 5 N and sliding speed of 1 m/s, with the contact being fully flooded in dodecane. In this high-speed condition, the flash temperature was estimated to be 150 °C. After the experiment, the tribofilm accumulated at the leading edge of the wear scar on the 52100 ball was examined by Raman spectroscopy after a short hexane rinse to remove residual dodecane, and after soaking for 24 h in dichloromethane (DCM), followed by a five-minute sonication in hexane to remove the remaining hydrocarbons. Raman spectroscopy was conducted with a Horiba LabRam HR Evolution confocal Raman microscope with the laser excitation wavelength of 473 nm, laser power of 1.25 mW and 100 × objective lens (NA = 0.95). The exposure time was 30 s and 3 accumulations.

As an independent test of the laser-induced degradation possibility, two organic compounds were analyzed with Raman spectroscopy (Horiba LabRam HR Evolution Vis–NIR). One was organic granulated cane sugar (Great Value, Walmart) purchased at a local grocery store, and the other was an air-dried inner bark of a poplar tree (~ 30 years old, dead) collected from a house yard at State College, PA.

2 Results and Discussion

Figure 1 shows the Raman spectra of tribofilms produced on SS during VPL of methylcyclopentane [37]. When irradiated with a low power laser (0.41mW) at 532 nm (= 2.33 eV photon energy, Fig. 1a), the tribofilm showed a large fluorescence background and negligible D- and G-bands. The fluorescence background means that the tribofilm absorbs the 532 nm irradiation and is excited electronically [60]. Electronic excitation in the visible wavelength is often observed for many aromatic hydrocarbons as well [61, 62]. It is possible that such aromatic components were produced and present in the tribofilm. When the 532 nm excitation laser power was increased to 2.05 mW, the D- and G-bands appeared prominent over the fluorescence background. At the same time, a burn mark could be seen in the illuminated spot (middle panel in Fig. 1a). When the laser power was reduced back to 0.41 mW, the D- and G-band features remained. This result clearly indicated that the D- and G-bands were induced by the high intensity laser beam via photochemical degradation. The laser power used in this study was comparable to the power of a simple commercial laser pointer; so it was quite low. But, when it was focused onto the sample with a 100 × objective lens, the power density was on the order of 10^5–10^6 W/cm^2. Heat diffusion calculations showed that the maximum temperature rise was only 47 K under these irradiation conditions [38] (see the Supporting Information for calculation detail). One might question whether the photochemical degradation was due to the photoelectron emission from the substrate. The work function of stainless steel is between 4.7 and 5.6 eV [63], which is far larger than the photon energy of 532 nm (2.3 eV). Thus, photoelectron emission is highly unlikely to occur under continuous wave (CW) laser irradiation at 532 nm.

The beam damage during Raman analysis is frequently mentioned in the literature [64, 65]. Even thick DLC or a-C films deposited via PECVD and PVD processes are prone to beam damage, which alters the relative intensity and peak positions of the D- and G- bands [66-69]. Note that it is the power density in the irradiated spot, not the power of the laser source, that is critical in determining whether beam damage will occur or not. Most Raman instruments focus the low-power laser beam to a small spot because typical Raman cross-sections of organic molecules are small,

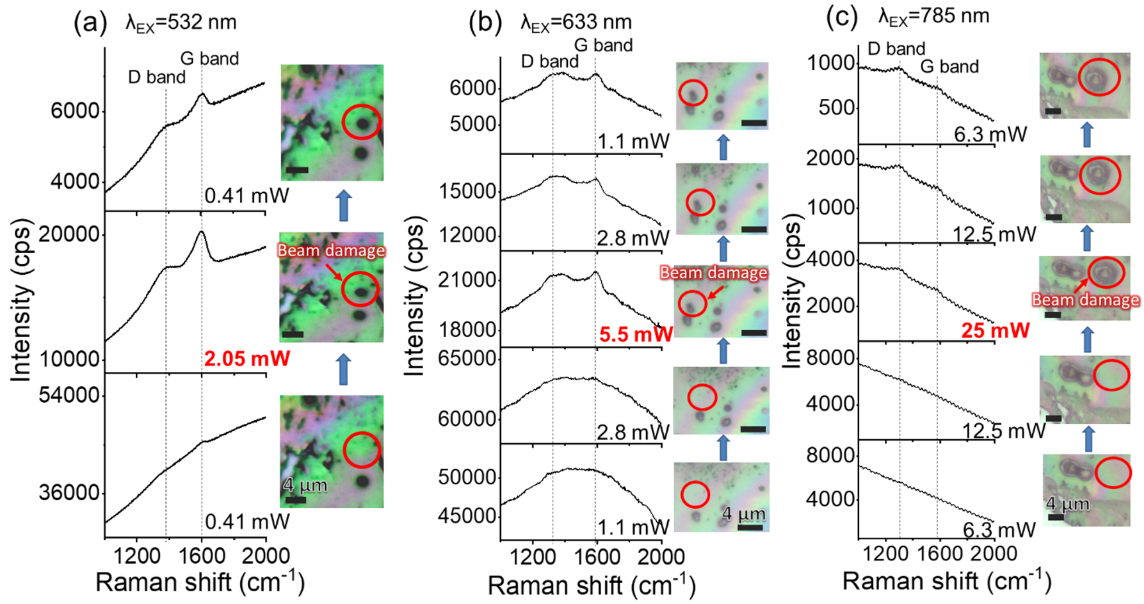

Fig. 1 **a** Evolution of D- and G-band features due to photochemical degradation of tribofilm produced on SS during VPL of methylcyclopentane. Results from experiments are shown progressing in time from bottom to top in these figures. The Raman analysis was done at the same location (marked with the red circles on the optical images) with λ_{EX} = 532 nm and varying laser power from 0.41 mW (1.0 × 10^5 W/cm^2) to 2.05 mW (5.0 × 10^5 W/cm^2), and then back to 0.41 mW, using a 100× objective lens (NA = 0.9). The data acquisition time was 10 s at each power. The thickness of the tribofilm marked with the red circle was ~ 1 µm. **b** The same measurements done with λ_{EX} = 633 nm and varying laser power from 1.1 mW (1.9 × 10^5 W/cm^2) to 5.5 mW (9.5 × 10^5 W/cm^2), and then back to 1.1 mW. **c** The same measurements done with λ_{EX} = 785 nm and varying laser power from 6.3 mW (7.0 × 10^5 W/cm^2) to 25 mW (28 × 10^5 W/cm^2), and then back to 6.3 mW. The undulating features in the spectra are due to the etaloning effect within the detector. The blue arrows indicate the order in which the Raman experiments were performed

and it also improves the collection efficiency of scattered Raman signals [40, 70]. This focusing can increase the power density in the irradiated spot above the beam damage threshold. For this reason, we have reported the laser power density in the irradiated spot in the captions of all figures.

A few studies provided sufficient information to calculate the laser power density at the analysis spot on tribofilms produced from organic precursors [11, 16]. The estimated power density was in the range of 3 × 10^5 W/cm^2 to 1 × 10^6 W/cm^2. When using λ_{EX} = 514.5 nm and a spot size of 1 µm, laser-induced damage on a-C:H film was observed at a power density of ~ 13 × 10^5 W/cm^2 with an exposure time of ~ 30 s [67]. When an UV laser (λ_{EX} = 244 nm) was used, it was suggested that the power density (assuming the spot size was 1 µm) should be kept below ~ 1 × 10^5 W/cm^2 to avoid beam damage, and the sample must be rotated at a very high speed (> 3000 rpm) to minimize beam damage due to a continuous exposure (up to 60 s) [66]. In our study, beam damage occurred when the power density reached 5.0 × 10^5 W/cm^2 when using the λ_{EX} = 532 nm with the exposure time of 1 s. At the same power density, the PECVD-deposited hydrogenated DLC film was also damaged, which was evident from the change of intensity of the D-band due to the sp^3 to sp^2 rehybridization of carbon induced by photochemical reactions [67] and the burn mark identifiable under the microscope. (See Figure S1 in Supporting Information).

To further support the hypothesis of photochemical degradation of tribofilms, we collected Raman spectra using longer wavelength excitations for tribofilms produced the same way as those analyzed above (Fig. 1b, c). When the photon energy was lowered from 532 nm (2.33 eV) to 633 nm (1.96 eV) and 785 nm (1.58 eV), the critical power needed to observe the appearance of the D- and G-bands was much higher. The difference in the baseline slope was due to the variation in fluorescence emission wavelength and detector sensitivity. There were no discernable D- and G-band features in the initial low-power spectra, and their appearance was accompanied by a burn mark on the sample surface. Once observed after irradiation at a high power, the D- and G-band features remained in the Raman spectra collected with a lower power at the same location. These results supported the hypothesis that the observed D- and G-band features from the tribofilm were due to photochemical degradation of triboproducts.

In the case of SS, the surface is covered with chromium oxide. Chromium oxide is known to be a catalyst for polymerization of olefins [71, 72]. However, even without such catalytically active surfaces, the tribofilm exhibiting the D- and G-band Raman spectral features can be produced. To

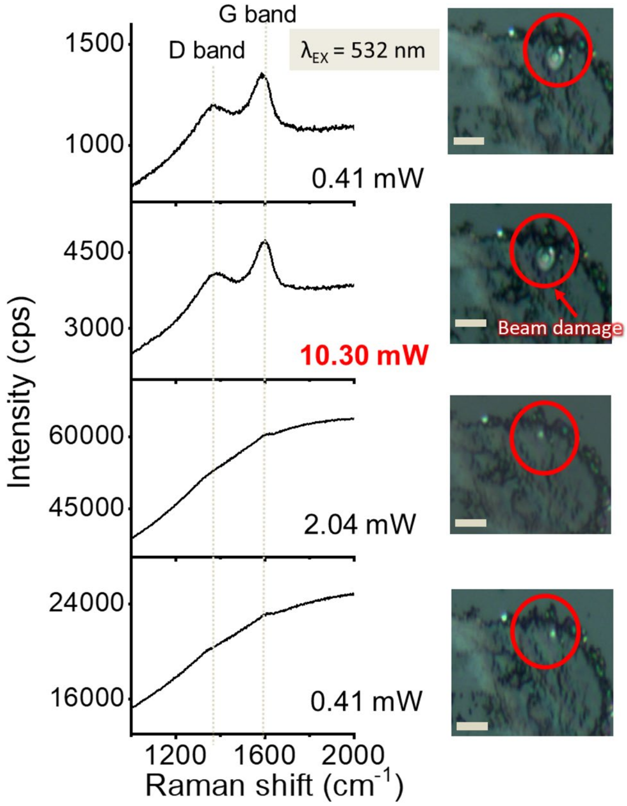

Fig. 2 **a** Evolution of the D- and G-bands in Raman spectra of the tribofilms produced on SLS glass during VPL of methylcyclopentane from the bottom to the top. The Raman analysis was done at the same location (marked with the red circles in the optical images) with λ_{EX} = 532 nm and varying laser power from 0.41 mW (1.0 × 10^5 W/cm^2) to 10.3 mW (25 × 10^5 W/cm^2), and then back to 0.41 mW (1.0 × 10^5 W/cm^2), using a 100× objective lens (NA = 0.9). The data acquisition time was 10 s at each power

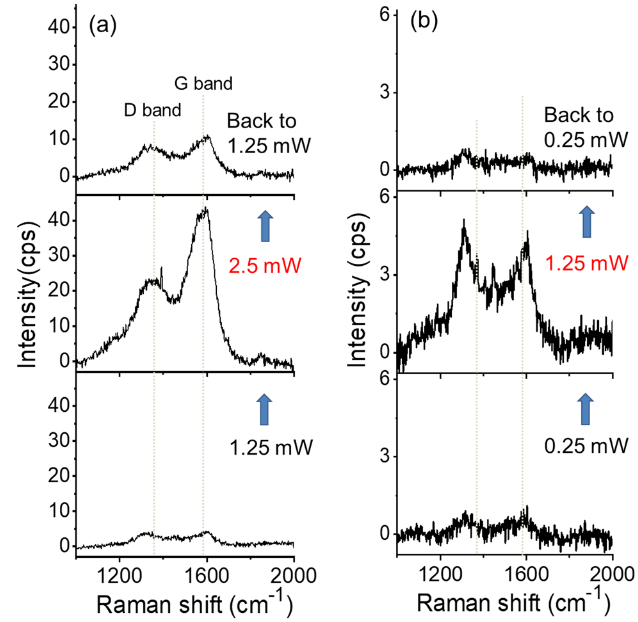

Fig. 3 **a** Raman spectra of the tribofilm remaining on a 52100-ball after tribo-testing against the 52100 flat at 2N load at a reciprocating frequency of 5 Hz for 1 h in PAO-4 oil. The spectra were collected at the same location with 473 nm excitation laser at a power of first 1.25 mW (4.5 × 10^5 W/cm^2), then 2.5 mW (9.0 × 10^5 W/cm^2), and then back to 1.25 mW (4.5 × 10^5 W/cm^2). **b** Raman spectra of the tribofilm at another location on the 52100-ball surface with a lower laser power (0.25 mW (0.9 × 10^5 W/cm^2) → 1.25 mW → 0.25 mW). The vertical lines are the positions of the D- and G-bands observed at 2.5 mW irradiation in **a**. Two sharp peaks at ~ 1400 cm^{-1} and ~ 1450 cm^{-1} are the C-H bending modes of the hydrocarbon-based lubricant oil. Note that the spectra shown here are after removal of the fluorescence background

test this hypothesis, we conducted the same VPL testing on 4 mm thick SLS glass (as an inert reference sample) and analyzed with Raman spectroscopy. The tribofilm formation yield on the SLS surface was about one tenth of that on the SS surface [56]. The threshold laser power needed to observe the D- and G-band features in the Raman spectrum was found to be higher for the tribofilm on SLS (Fig. 2) than for the tribofilm on SS (Fig. 1a). The most likely reason is that SLS is transparent at 532 nm and its refractive index is close to the values of most organic materials, while SS is reflective. In other words, the tribofilm on the SLS surface would experience less photon exposure than the SS surface at the same irradiation condition.

The tribofilms formed under the PAO-4 liquid lubrication condition showed the same photochemical degradation behavior as seen in the VPL experiments when the excitation laser power was high enough. Figure 3a reveals the variation of Raman spectra obtained at a fixed spot on the tribofilm with respect to the laser power. Raman measurements were conducted at 1.25 mW (4.5 × 10^5 W/cm^2), followed by 2.5 mW (9.0 × 10^5 W/cm^2), and then by 1.25 mW (4.5 × 10^5 W/cm^2) again. At the initial 1.25 mW irradiation, the D- and G-band intensities were around 3 and 5 cps, respectively, after removal of the background. Upon subjecting the same spot to 2.5 mW, their intensities rose to ~ 20 and ~ 42 cps, respectively. When repeated at 1.25 mW laser power again, the same spot yielded D- and G-band intensities of ~ 7 and ~ 10 cps, respectively. Figure 3b shows the same analysis done at a different spot with laser power starting at 0.25 mW (0.9 × 10^5 W/cm^2), followed by 1.25 mW (4.5 × 10^5 W/cm^2), and then back to 0.25 mW again. The fact that similar signatures were obtained at 0.25 mW laser power before and after the exposure to 1.25 mW laser power indicates that the degree of photochemical degradation was relatively small at this low power condition. Note, however, that the Raman band positions and their relative intensities obtained at 0.25 and 1.25 mW (Fig. 3b) are different from those obtained at 2.5 mW (Fig. 3a), suggesting that the chemical nature of the original tribofilm is different from that induced by high-power laser irradiation. In summary, these results confirm

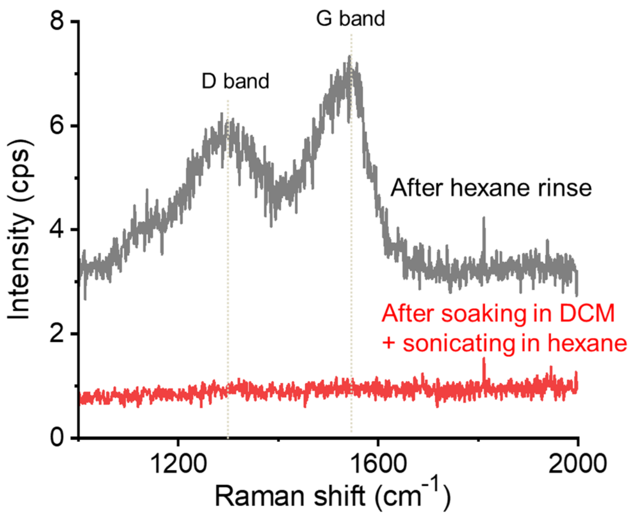

Fig. 4 Raman spectra of the tribofilm remaining on a 52100 ball (after hexane rinse and after soaking in DCM for 24 h + sonicating in hexane for 5 min) after tribo-testing against the D2 steel at 5N load at a sliding speed of 1 m/s for 5 h in dodecane. The spectra were collected with 473 nm excitation laser at a power of 1.25 mW (4.5 × 10^5 W/cm.^{2}) using a 100 × objective lens (NA = 0.95)

that sufficiently high-power laser radiation can induce photochemical degradation of the tribofilm formed from PAO-4.

High-speed (1 m/s) ball-on-disk tribotest was conducted to determine if a DLC or a-C film could be formed tribochemically under more severe experimental conditions. In this case, the average flash temperature was estimated to be about 150 °C above the ambient temperature [59] (see the Supporting Information). The tribofilm formed after such tribotests showed two broad peaks around 1300 cm^{-1} and 1580 cm^{-1} (Fig. 4), which are similar to the Raman *D* and *G* band signatures of DLC or a-C. However, after soaking the tribofilm in DCM for 24 h, followed by a short sonication in hexane, these bands disappeared. The dissolution of the tribofilm in DCM suggests that the tribofilm is not DLC or a-C. Instead, the tribofilm formed under this harsher condition might be a mixture of various oligomeric species.

The photochemical degradation caused by the high-intensity laser beam during the Raman analysis suggests that tribochemically produced organic species are photochemically unstable. When a thin film of polystyrene (PS) was deposited on pristine SS and SLS surfaces and the Raman analysis was conducted with the 532 nm excitation at 10.3 mW (25 × 10^5 W/cm^2), the vibrational spectral features of PS did not

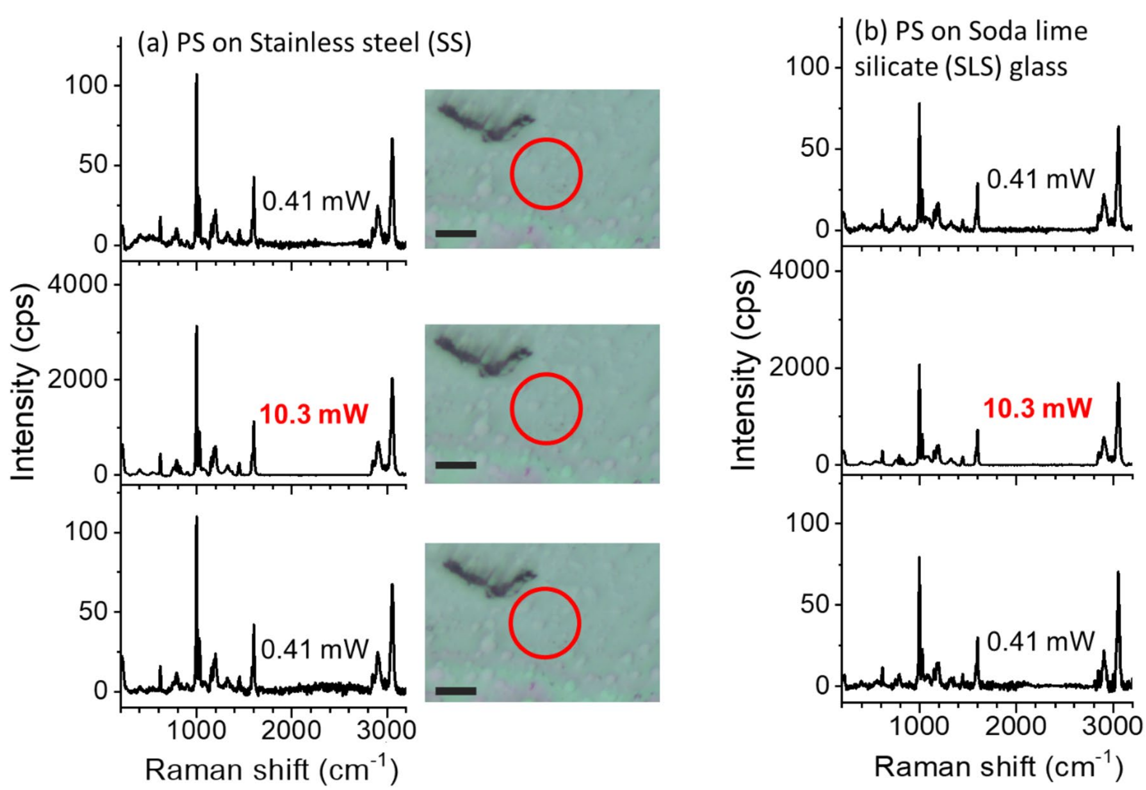

Fig. 5 Raman spectra of a 300 nm thick polystyrene (PS) film dip-coated on (**a**) SS or (**b**) SLS substrates. The Raman analysis was done at the same location (marked with the red circles on optical images) with λ_{EX} = 532 nm and under varying laser power from 0.41 mW (1.0 × 10^5 W/cm^2) to 10.3 mW (25 × 10^5 W/cm^2), and then back to 0.41 mW, using a 100 × objective lens (NA = 0.9). The data acquisition time was 10 s at each power. In the case of PS/SLS, no optical image was taken since the substrate was not visible

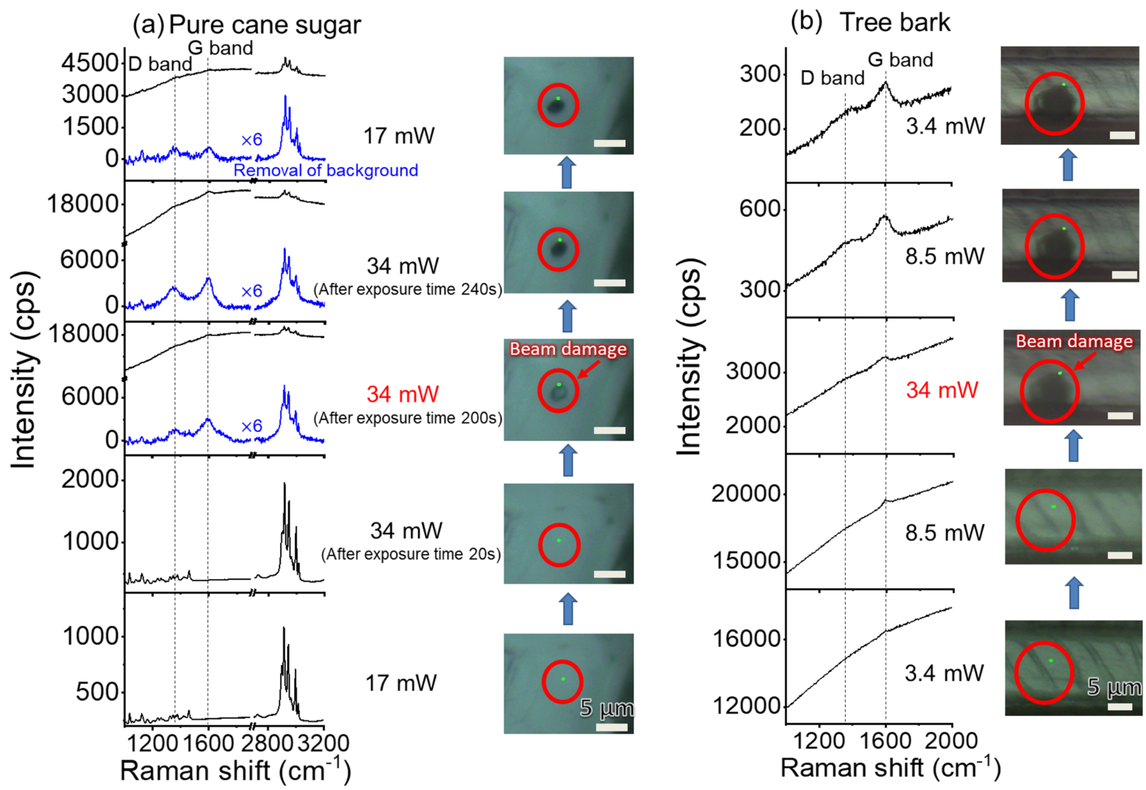

Fig. 6 Evolution of the D- and G-bands in the Reman spectra of (**a**) granulated cane sugar and (**b**) poplar bark. The Raman analysis was done at the same location (marked with the red circles on optical images, and the green dot indicates the measurement point) with $\lambda_{EX}=532$ nm and under varying laser power. Objective lens of 100×(NA = 0.9) and 50×(NA = 0.5) were used to focus laser beams on sugar cane granule and polar bark, respectively. The cane sugar was damaged after being exposed to the 34 mW (82×10^5 W/cm^2) laser for 220 s, while the tree bark was damaged when it was exposed to the 34 mW (33×10^5 W/cm^2) laser for 10 s. The blue lines in the Raman spectra of cane sugar were obtained by subtracting the background from the raw spectra

change at all, indicating that PS did not degrade at this high-power irradiation condition (Fig. 5). Note that the baseline of the PS Raman spectrum is quite flat, indicating that there is no electronic excitation. In the UV–VIS absorption spectrum, PS shows a peak around 270 nm (which corresponds to 4.6 eV) [73, 74]. Thus, its photochemical activity is negligible at 532 nm irradiation. In comparison, the tribofilms studied here absorbed the 532 nm laser beam and fluoresced (Figs. 1 and 2). Such electronic excitation and subsequent relaxation processes are likely to be accompanied by photochemical degradation reactions [75] that occur more readily at shorter-wavelength laser excitation [64].

Note that the excitation laser beam used for the Raman analysis can degrade even stable compounds if the laser power is sufficiently high. To demonstrate this, we did a series of control experiments with a granule of cane sugar and the inner bark of a poplar tree. Figure 6 shows the Raman spectra of cane sugar and tree bark collected at high laser powers. When cane sugar was irradiated with 17 mW (41×10^5 W/cm^2) of 532 nm excitation laser (Fig. 6a), the collected Raman spectrum was in good agreement with that found in the literature (see the Supporting Information) and did not change over time [76]. When the laser power was increased to 34 mW (82×10^5 W/cm^2), the sharp molecular vibration features disappeared gradually, and a broad fluorescent background grew over time. Eventually, weak but clearly noticeable D- and G-band features appeared on top of the fluorescent background. After subtracting the background of the raw spectra, apparent D- and G- bands were observed. Similar to the tribofilm case, this appearance was accompanied by a burn mark (beam damage) on the sample surface. In this case, it is possible that the degradation process was thermochemical. Assuming the thermal conductivity of sugar is 0.15 W/m–K [77, 78] and the absorption cross section is 0.01 [79], the maximum temperature inside the focused beam of 532 nm at 34 mW could reach ~ 1300 K when focused with the 100×(NA = 0.9) objective lens. Initially, the degradation must be of thermal origin because there was no fluorescence detected prior to beam damage. After the onset of thermal decomposition, the products could undergo photochemical degradation as well, accelerating further degradation. Thus, it is likely that the beam damage has both thermal and photochemical processes, which eventually leads to significant changes in the spectrum.

In the case of the poplar bark (Fig. 6b), only a broad fluorescence background signal was detected at 3.4 mW (3.3×10^5 W/cm^2) irradiation. This must be due to the autofluorescence of lignin components in the bark [80, 81]. At 34 mW (33×10^5 W/cm^2), a clear burn mark was observed, and the D- and G-bands appeared in the Raman spectrum. Because pyrolysis of tree bark is known to produce active carbon materials [82, 83], a similar degradation process is expected under the high-intensity laser irradiation, producing the D- and G-band features in the collected spectrum. Therefore, it is possible that thermochemical degradation reactions can also take place when conducting Raman experiment at high laser power.

During the literature review, we noted that many papers reported Raman spectra *after background removal* to show the D- and G-bands clearly (similar to those shown in Figs. 3 and 4; the raw Raman spectrum of another sample without background subtraction is shown in Figure S3 in the Supporting Information) [11-28, 30-38, 84-86]. The fluorescence background in the Raman spectrum gives important structural information. If the tribofilm is truly DLC, a-C, or graphitic material, the fluorescence background could be related to the hydrogen content in the amorphous carbon network [87]. The results of this study, however, revealed that, for the examples analyzed here, a strong fluorescence background could be produced by unstable organic molecules that absorb the excitation laser beam of Raman analysis and undergo photochemical degradation. The Raman cross-sections of organic hydrocarbon molecules are relatively small [40, 88], so it is difficult to observe their molecular vibrational spectral features when the fluorescence background is high. Therefore, in Raman analysis of aromatic compounds, the excitation wavelength is carefully chosen to avoid such fluorescence background [65]. In the absence of clearly identifiable molecular features in the spectrum collected with a low laser power, one may increase the laser power until some identifiable spectral features appear. However, as shown in Figs. 1–3 and 6, those spectral features observed under the high-power-density laser irradiation cannot be assumed to be the features of the pristine sample unless the possibility of beam damage is ruled out.

All a-C and graphitic materials show D- and G-bands in Raman; even cokes and carbon soot produced by thermal degradation of organics show the same D- and G-band features [41, 42, 51, 64, 89-91]. In addition, many carbonaceous materials exhibit Raman peaks near the D- and G- band peak positions [23, 92-94], and a change in the D- and G- band peak intensities was also observed between oxidized and non-oxidized samples of carbonaceous material [95]. Thus, the observation of the D- and G-bands in Raman spectra of tribofilms may not be sufficient to claim that the tribofilm produced was DLC, a-C, or graphitic species or contains such components.

Other complementary and non-destructive characterization methods should be employed to test and confirm if DLC, a-C, or graphitic species are produced indeed by tribochemical processes, and such methods should be free from the beam damage during the analysis [64, 96-100]. Such techniques include infrared spectroscopy for detection of organic functional groups [37, 101, 102], matrix-assisted laser desorption/ionization mass spectrometry (MALDI-MS) or secondary ion mass spectrometry (SIMS) for molecular weight distribution [18, 25, 56, 103, 104], x-ray photoelectron spectroscopy (XPS) for elemental analysis [28, 101, 105-108], x-ray absorption near edge structure (XANES) or electron energy loss spectroscopy (EELS) for carbon hybridization [18, 25, 27, 101, 104-106, 108], transmission electron spectroscopy (TEM) for imaging [18, 21, 32, 35, 101], and so on. However, it should be noted that each technique has its own limitations. Although IR is known to be molecular-specific, it would be difficult to differentiate individual species if the tribofilm contains many different chemical species. MALDI and SIMS suffer from fragmentation during the ionization, although the fragmentation pattern could be specific to certain molecular patterns [56]. If the tribofilm is not stable, it could get oxidized upon exposure to air during the sample transfer, which may alter the XPS elemental analysis result [109] During the XANES analysis at C K-edge, the high intensity x-ray beam can degrade the sample [110-112]. Similarly, organic materials are highly susceptible to beam damage under high-energy electron irradiation during TEM and EELS analysis unless specific care is taken to reduce beam damage [113, 114]. If graphitic domains are present in the sample, they could be found and imaged with TEM; but without proper statistics or concentration information, it would be difficult to fully evaluate the importance of their presence. Since no single technique can provide sufficient information, the use of multiple techniques with proper knowledge of experimental artifacts and limitations of each technique is critically needed to better and more accurate characterization of tribofilms which are inherently complex due to the lack of reaction specificity under highly dynamic and non-equilibrium conditions of tribological interfaces [37, 115].

3 Conclusions

A possible origin of the D- and G-band features in the Raman spectra of tribofilms produced by tribochemical reactions was explored. While the D- and G- bands in the Raman spectrum can serve as an indicator of the presence of DLC or a-C films, it is important to delineate the origin of such D- and G- bands in the spectrum. Control studies conducted with varying laser powers and wavelengths indicated that such spectral features can be produced by beam damage during the Raman analysis. This finding suggests that the hypothesis of synthesizing DLC, a-C, or graphitic species by friction solely based on the observation of D- and G-bands in Raman spectra needs to be confirmed with complementary characterization methods that do not cause degradation of tribofilms during the analysis.

Supplementary Information The online version contains supplementary material available at https://doi.org/10.1007/s11249-023-01728-1.

Acknowledgements This work was supported by the National Science Foundation: Penn Stat work was through Grant No. CMMI-1912199, CMMI-2038494, and DMR-2011410, the UC Merced work was through CMMI-2038499, and the Northwestern work was through CMMI-1662606. Also, the Northwestern work was partially supported by Army Research Laboratory Vehicle Technology Directorate (VTD) under Cooperative Agreement Number W911NF-20-2-0292. The authors appreciated the comments made by reviewers to clarify the main message of this paper for the tribology and tribochemistry community.

Author contributions All authors contributed to the study's conception and design, and to the writing. Material preparation, data collection, and analysis were performed by Yu-Sheng Li, Seokhoon Jang, Arman Khan, Tobias Martin, and Andrew L. Ogrinc. Seong H. Kim, Ashlie Martini, Yip-Wah Chung, and Q. Jane Wang supervised the study and provided critical feedback, and helped to revise the manuscript. All authors read and approved the final manuscript

Funding National Science Foundation, CMMI-2038494, CMMI-1912199, CMMI-1662606, DMR-2011410, Army Research Laboratory Vehicle Technology Directorate (VTD), W911NF-20-2-0292

Data availability The authors of this study have affirmed that the data which supports their findings can be found in the paper and its Supplementary Information files. Data sets generated during the current study are available from the corresponding author upon reasonable request.

Declarations

Conflict of interest The authors declare no competing financial interest.

References

1. Fischer, T.: Tribochemistry. Annu. Rev. Mater. Sci. **18**, 303–323 (1988)
2. Hsu, S.M., Zhang, J., Yin, Z.: The nature and origin of tribochemistry. Tribol. Lett. **13**, 131–139 (2002). https://doi.org/10.1023/A:1020112901674
3. Chen, Y., Renner, P., Liang, H.: A review of current understanding in tribochemical reactions involving lubricant additives. Friction (2022). https://doi.org/10.1007/s40544-022-0637-2
4. Carlton, H., Huitink, D., Liang, H.: Tribochemistry as an alternative synthesis pathway. Lubricants **8**, 87 (2020)
5. He, X., Ngo, D., Kim, S.H.: Mechanochemical Reactions of Adsorbates at Tribological Interfaces: Tribopolymerizations of Allyl Alcohol Coadsorbed with Water on Silicon Oxide. Langmuir **35**, 15451–15458 (2019). https://doi.org/10.1021/acs.langmuir.9b01663
6. Palacios, J.: Films formed by antiwear additives and their incidence in wear and scuffing. Wear **114**, 41–49 (1987)
7. Luiz, J.F., Spikes, H.: Tribofilm formation, friction and wear-reducing properties of some phosphorus-containing antiwear additives. Tribol. Lett. **68**, 1–24 (2020)
8. He, X., Pollock, A., Kim, S.H.: Effect of Gas environment on mechanochemical reaction: A model study with tribo-polymerization of α-pinene in inert, oxidative, and reductive gases. Tribol. Lett. (2019). https://doi.org/10.1007/s11249-019-1136-0
9. He, X., Kim, S.H.: Mechanochemistry of physisorbed molecules at tribological interfaces: molecular structure dependence of tribochemical polymerization. Langmuir **33**, 2717–2724 (2017)
10. Fujita, H., Spikes, H.: The formation of zinc dithiophosphate antiwear films. Proceedings of the Institution of Mechanical Engineers, Part J: Journal of Engineering Tribology **218**, 265–278 (2004)
11. Herrera-Fierro, P., Shogrin, B.A., Jones Jr, W.R. (1996) Spectroscopic Analysis of Perfluoropolyether Lubricant Degradation During Boundary Lubrication. Tribology Conference. Place
12. Cheng, U.C., Stair, P.C.: In situ study of multialkylated cyclopentane and perfluoropolyalkyl ether chemistry in concentrated contacts using ultraviolet Raman spectroscopy. Tribol. Letters **4**, 163–170 (1998). https://doi.org/10.1023/A:1019147020100
13. John, P., Cutler, J., Sanders, J.: Tribological behavior of a multialkylated cyclopentane oil under ultrahigh vacuum conditions. Tribol. Lett. **9**, 167–173 (2001). https://doi.org/10.1023/A:1018808921623
14. Liao, Y., Pourzal, R., Wimmer, M., Jacobs, J., Fischer, A., Marks, L.: Graphitic tribological layers in metal-on-metal hip replacements. Science **334**, 1687–1690 (2011)
15. de Figueiredo, M.R., Bergmann, C., Ganser, C., Teichert, C., Kukla, C., Mitterer, C.: Adhesion tendency of polymers to hard coatings. Int. Polym. Proc. **28**, 415–420 (2013)
16. Khaemba, D.N., Neville, A., Morina, A.: A methodology for Raman characterisation of MoDTC tribofilms and its application in investigating the influence of surface chemistry on friction performance of MoDTC lubricants. Tribol. Lett. **59**, 1–17 (2015). https://doi.org/10.1007/s11249-015-0566-6
17. Wimmer, M., Laurent, M., Mathew, M., Nagelli, C., Liao, Y., Marks, L., et al.: The effect of contact load on CoCrMo wear and the formation and retention of tribofilms. Wear **332**, 643–649 (2015). https://doi.org/10.1016/j.wear.2015.02.013
18. Erdemir, A., Ramirez, G., Eryilmaz, O.L., Narayanan, B., Liao, Y., Kamath, G., et al.: Carbon-based tribofilms from lubricating oils. Nature **536**, 67–71 (2016). https://doi.org/10.1038/nature18948
19. Johnson, B., Wu, H., Desanker, M., Pickens, D., Chung, Y.-W., Jane Wang, Q.: Direct formation of lubricious and wear-protective carbon films from phosphorus- and sulfur-free oil-soluble additives. Tribol. Letters (2017). https://doi.org/10.1007/s11249-017-0945-2
20. Miyajima, M., Kitamura, K., Matsumoto, K.: Characterization of tribochemical reactions on steel surfaces. Nippon Steel Sumitomo Met Tech Rep **114**, 101–107 (2017)
21. Argibay, N., Babuska, T., Curry, J., Dugger, M., Lu, P., Adams, D., et al.: In-situ tribochemical formation of self-lubricating diamond-like carbon films. Carbon **138**, 61–68 (2018). https://doi.org/10.1016/j.carbon.2018.06.006
22. Pham, S.T., Wan, S., Tieu, K.A., Ma, M., Zhu, H., Nguyen, H.H., et al.: Unusual competitive and synergistic effects of graphite nanoplates in engine oil on the tribofilm formation. Adv. Mater. Interfaces **6**, 1901081 (2019). https://doi.org/10.1002/admi.201901081

23. Wu, H., Khan, A.M., Johnson, B., Sasikumar, K., Chung, Y.W., Wang, Q.J.: Formation and nature of carbon-containing tribofilms. ACS Appl Mater Interfaces **11**, 16139–16146 (2019). https://doi.org/10.1021/acsami.8b22496
24. Khan, A.M., Wu, H., Ma, Q., Chung, Y.-W., Wang, Q.J.: Relating tribological performance and tribofilm formation to the adsorption strength of surface-active precursors. Tribol Letters (2019). https://doi.org/10.1007/s11249-019-1249-5
25. Deng, Q., Gong, Y., Jing, P., Ma, D., Li, Y., Ye, T., et al.: Formation of a carbonaceous film on the surface of Cu in a bovine serum albumin solution. Surf. Coat. Technol. **358**, 611–616 (2019). https://doi.org/10.1016/j.surfcoat.2018.11.095
26. Ma, Q., Khan, A.M., Wang, Q.J.: Dependence of tribological performance and tribopolymerization on the surface binding strength of selected cycloalkane-carboxylic acid additives. Tribol. Lett. **68**, 1–10 (2020). https://doi.org/10.1007/s11249-020-01329-2
27. Ramirez, G., Eryilmaz, O.L., Fatti, G., Righi, M.C., Wen, J., Erdemir, A.: Tribochemical conversion of methane to graphene and other carbon nanostructures: implications for friction and wear. ACS Applied Nano Materials **3**, 8060–8067 (2020). https://doi.org/10.1021/acsanm.0c01527
28. Zhang, R., Chen, Q., Fan, X., He, Z., Xiong, L., Shen, M.: In situ friction-induced graphene originating from methanol at the sliding interface between the WC self-mated tribo-pair and its tribological performance. Langmuir **36**, 3887–3893 (2020). https://doi.org/10.1021/acs.langmuir.9b03963
29. Xu, X., Xu, Z., Sun, J., Tang, G., Su, F.: In situ synthesizing carbon-based film by tribo-induced catalytic degradation of poly-α-olefin oil for reducing friction and wear. Langmuir **36**, 10555–10564 (2020). https://doi.org/10.1021/acs.langmuir.0c01896
30. Huynh, K.K., Tieu, K.A., Pham, S.T.: Synergistic and competitive effects between zinc dialkyldithiophosphates and modern generation of additives in engine oil. Lubricants **9**, 35 (2021). https://doi.org/10.3390/lubricants9040035
31. Adachi, K.: Superlubricity of carbon nitride coatings in inert gas environments, pp. 189–214. Superlubricity, Elsevier Amsterdam (2021)
32. Kabel, J., Edwards, T.E.J., Hain, C., Kochetkova, T., Parkison, D., Michler, J., et al.: A novel fiber-fretting test for tribological characterization of the fiber/matrix interface. Compos. Part B: Eng. (2021). https://doi.org/10.1016/j.compositesb.2020.108535
33. Shirani, A., Li, Y., Eryilmaz, O.L., Berman, D.: Tribocatalytically-activated formation of protective friction and wear reducing carbon coatings from alkane environment. Sci. Rep. **11**, 1–9 (2021). https://doi.org/10.1038/s41598-021-00044-9
34. Fu, X., Cao, L., Wan, Y., Li, R.: Superlubricity achieved with TiN coatings via the in situ formation of a carbon-based film at the sliding interfaces. Ceram. Int. **47**, 33917–33921 (2021). https://doi.org/10.1016/j.ceramint.2021.08.229
35. Kohlhauser, B., Vladu, C.I., Gachot, C., Mayrhofer, P.H., Ripoll, M.R.: Reactive in-situ formation and self-assembly of MoS2 nanoflakes in carbon tribofilms for low friction. Mater. Design **199**, 109427 (2021). https://doi.org/10.1016/j.matdes.2020.109427
36. Zhang, J., Campen, S., Wong, J., Spikes, H.: Oxidational wear in lubricated contacts–Or is it? Tribol Int. **165**, 107287 (2022). https://doi.org/10.1016/j.triboint.2021.107287
37. Li, Y.-S., Jang, S., Bhuiyan, F.H., Martini, A., Kim, S.H.: Molecular structure and environment dependence of shear-driven chemical reactions: Comparative study of tribopolymerization of methylcyclopentane, cyclohexane and cyclohexene on stainless steel. Tribol. Lett. (2023). https://doi.org/10.1007/s11249-023-01703-w
38. Khan, A.M., Ahmed, J., Liu, S., Martin, T., Berkebile, S., Chung, Y.-W., et al.: Formation of wear-protective tribofilms on different steel surfaces during lubricated sliding. Tribol Lett. (2022). https://doi.org/10.21203/rs.3.rs-2645494/v1
39. Orlando, A., Franceschini, F., Muscas, C., Pidkova, S., Bartoli, M., Rovere, M., et al.: A comprehensive review on Raman spectroscopy applications. Chemosensors **9**, 262 (2021)
40. Smith, E., Dent, G.: Modern Raman Spectroscopy A Practical Approach. John Wiley & Sons, West Sussex, England (2005)
41. Ferrari, A., Robertson, J., Benedek, G., Milani, P., Ralchenko, V.: Nanostructured carbon for advanced applications. J Nano Car Adv Appl **24**, 177 (2001). https://doi.org/10.1007/978-94-010-0858-7
42. Ferrari, A.C., Robertson, J.: Interpretation of Raman spectra of disordered and amorphous carbon. Phys. Rev. B **61**, 14095 (2000). https://doi.org/10.1103/PhysRevB.61.14095
43. Erdemir, A., Eryilmaz, O., Nilufer, I., Fenske, G.: Synthesis of superlow-friction carbon films from highly hydrogenated methane plasmas. Surf. Coat. Technol. **133**, 448–454 (2000). https://doi.org/10.1016/S0257-8972(00)00968-3
44. Erdemir, A., Donnet, C.: Tribology of diamond-like carbon films: recent progress and future prospects. J. Phys. D Appl. Phys. **39**, R311 (2006)
45. Jeng, Y.R., Islam, S., Wu, K.T., Erdemir, A., Eryilmaz, O.: Investigation of nano-mechanical and- tribological properties of hydrogenated diamond like carbon (DLC) coatings. J. Mech. **33**, 769–776 (2016). https://doi.org/10.1017/jmech.2016.106
46. Jang, S., Chen, Z., Kim, S.H.: Environmental effects on superlubricity of hydrogenated diamond-like carbon: Understanding tribochemical kinetics in O_2 and H_2O environments. Appl. Surf. Sci. (2022). https://doi.org/10.1016/j.apsusc.2021.152299
47. Li, H., Xu, T., Wang, C., Chen, J., Zhou, H., Liu, H.: Friction behaviors of hydrogenated diamond-like carbon film in different environment sliding against steel ball. Appl. Surf. Sci. **249**, 257–265 (2005). https://doi.org/10.1016/j.apsusc.2004.12.002
48. Manimunda, P., Al-Azizi, A., Kim, S.H., Chromik, R.R.: Shear-induced structural changes and origin of ultralow friction of hydrogenated diamond-like carbon (DLC) in dry environment. ACS Appl. Mater. Interfaces **9**, 16704–16714 (2017). https://doi.org/10.1021/acsami.7b03360
49. Donnet, C., Erdemir, A.: Tribology of diamond-like carbon films: Fundamentals and applications. Springer, Berlin (2007)
50. Johnson, J.A., Woodford, J.B., Rajput, D., Kolesnikov, A.I., Schleuter, J.A., Eryilmaz, O.L., et al.: Carbon-hydrogen bonding in near-frictionless carbon. Appl. Phys. Lett. **93**, 131911 (2008). https://doi.org/10.1063/1.2990757
51. Lajaunie, L., Pardanaud, C., Martin, C., Puech, P., Hu, C., Biggs, M., et al.: Advanced spectroscopic analyses on a: CH materials: Revisiting the EELS characterization and its coupling with multi-wavelength Raman spectroscopy. Carbon **112**, 149–161 (2017)
52. Guizani, C., Haddad, K., Limousy, L., Jeguirim, M.: New insights on the structural evolution of biomass char upon pyrolysis as revealed by the Raman spectroscopy and elemental analysis. Carbon **119**, 519–521 (2017)
53. Ko, T.H., Kuo, W.S., Chang, Y.H.: Raman study of the microstructure changes of phenolic resin during pyrolysis. Polym. Compos. **21**, 745–750 (2000)
54. Schuepfer, D.B., Badaczewski, F., Guerra-Castro, J.M., Hofmann, D.M., Heiliger, C., Smarsly, B., et al.: Assessing the structural properties of graphitic and non-graphitic carbons by Raman spectroscopy. Carbon **161**, 359–372 (2020)
55. Zahra, H., Sawada, D., Kumagai, S., Ogawa, Y., Johansson, L.-S., Ge, Y., et al.: Evolution of carbon nanostructure during pyrolysis of homogeneous chitosan-cellulose composite fibers. Carbon **185**, 27–38 (2021)

56. He, X., Barthel, A.J., Kim, S.H.: Tribochemical synthesis of nano-lubricant films from adsorbed molecules at sliding solid interface: Tribo-polymers from α-pinene, pinane, and n-decane. Surf. Sci. **648**, 352–359 (2016). https://doi.org/10.1016/j.susc.2016.01.005
57. Barthel, A.J., Combs, D.R., Kim, S.H.: Synthesis of polymeric lubricating films directly at the sliding interface via mechanochemical reactions of allyl alcohols adsorbed from the vapor phase. RSC Adv **4**, 26081–26086 (2014). https://doi.org/10.1039/c4ra02283a
58. Bhuiyan, F.H., Li, Y.-S., Kim, S.H., Martini, A.: Shear-activated chemisorption and association of cyclic organic molecules. Faraday Discuss. (2023). https://doi.org/10.1039/d2fd00086
59. Ashby, M., Abulawi, J., Kong, H.: Temperature maps for frictional heating in dry sliding. Tribol. Trans. **34**, 577–587 (1991). https://doi.org/10.1080/10402009108982074
60. Van Duuren, B.: The fluorescence spectra of aromatic hydrocarbons and heterocyclic aromatic compounds. Anal. Chem. **32**, 1436–1442 (1960)
61. Bejaoui, S., Mercier, X., Desgroux, P., Therssen, E.: Laser induced fluorescence spectroscopy of aromatic species produced in atmospheric sooting flames using UV and visible excitation wavelengths. Combust. Flame **161**, 2479–2491 (2014)
62. Li, G.Y., Han, K.L.: The sensing mechanism studies of the fluorescent probes with electronically excited state calculations. Wiley Interdisciplinary Reviews: Computational Molecular Science **8**, e1351 (2018). https://doi.org/10.1002/wcms.1351
63. Surplice, N., D'Arcy, R.: Reduction in the work function of stainless steel by electric fields. J. Phys. F: Met. Phys. **2**, L8 (1972)
64. Chua, Y.T., Stair, P.C.: A novel fluidized bed technique for measuring UV Raman spectra of catalysts and adsorbates. J. Catal. **196**, 66–72 (2000). https://doi.org/10.1006/jcat.2000.3017
65. Agarwal, U.P.: 1064 nm FT-Raman spectroscopy for investigations of plant cell walls and other biomass materials. Front. Plant Sci. **5**, 490 (2014). https://doi.org/10.3389/fpls.2014.00490
66. Ferrari, A.C., Robertson, J.: Resonant Raman spectroscopy of disordered, amorphous, and diamondlike carbon. Phys. Rev. B **64**, 075414 (2001). https://doi.org/10.1103/PhysRevB.64.075414
67. Lamberton, R., Morley, S., Maguire, P., McLaughlin, J.: Monitoring laser-induced microstructural changes of thin film hydrogenated amorphous carbon (aC: H) using Raman spectroscopy. Thin Solid Films **333**, 114–125 (1998). https://doi.org/10.1016/S0040-6090(98)00848-7
68. Nistor, L.C., Van Landuyt, J., Ralchenko, V., Kononenko, T., Obraztsova, E.D., Strelnitsky, V.: Direct observation of laser-induced crystallization of aC: H films. Appl. Phys. A **58**, 137–144 (1994). https://doi.org/10.1007/BF00332170
69. Casiraghi, C., Ferrari, A., Robertson, J.: Raman spectroscopy of hydrogenated amorphous carbons. Phys. Rev. B **72**, 085401 (2005). https://doi.org/10.1103/PhysRevB.72.085401
70. Stephenson, D.A.: Raman cross sections of selected hydrocarbons and freons. J. Quant. Spectrosc. Radiat. Transfer **14**, 1291–1301 (1974). https://doi.org/10.1016/0022-4073(74)90098-3
71. Ayscough, P., Eden, C., Steiner, H.: Polymerization of ethylene over supported chromium oxide catalysts. J. Catal. **4**, 278–290 (1965)
72. Hogan, J.: Ethylene polymerization catalysis over chromium oxide. J. Polym. Sci. A-1 Polym. Chem. (1970). https://doi.org/10.1002/pol.1970.150080929
73. Li, T., Zhou, C., Jiang, M.: UV absorption spectra of polystyrene. Polym. Bull. **25**, 211–216 (1991)
74. Jaleh, B., Madad, M.S., Tabrizi, M.F., Habibi, S., Golbedaghi, R., Keymanesh, M.: UV-degradation effect on optical and surface properties of polystyrene-TiO2 nanocomposite film. J. Iran. Chem. Soc. **8**, S161–S168 (2011)
75. Schinke, R.: Photodissociation dynamics: spectroscopy and fragmentation of small polyatomic molecules. Cambridge University Press, Cambridge (1995)
76. Dahlenborg, H., Millqvist-Fureby, A., Brandner, B.D., Bergenstahl, B.: Study of the porous structure of white chocolate by confocal Raman microscopy. Eur. J. Lipid Sci. Technol. **114**, 919–926 (2012). https://doi.org/10.1002/ejlt.201200006
77. Cuevas, R., Cheryan, M.: Thermal conductivity of liquid foods—A review. J. Food Process Eng **2**, 283–306 (1978)
78. Mattea, M., Urbicain, M., Rotstein, E.: Prediction of thermal conductivity of vegetable foods by the effective medium theory. J. Food Sci. **51**, 113–115 (1986)
79. Carlslaw, H., Jaeger, J.: Conduction of heat in solids. Oxford University Press, Oxford (1959)
80. Radoykova, T.H., Radeva, G.V., Nenkova, S.K.: Comparative kinetic analysis of poplar biomass alkaline hydrolysis. Cellul. Chem. Technol. **50**, 269–274 (2016)
81. Donaldson, L.: Autofluorescence in plants. Molecules **25**, 2393 (2020)
82. Zhang, J., Zhang, W.: Preparation and characterization of activated carbon fibers from liquefied poplar bark. Mater. Lett. **112**, 26–28 (2013)
83. Momodu, D., Madito, M., Barzegar, F., Bello, A., Khaleed, A., Olaniyan, O., et al.: Activated carbon derived from tree bark biomass with promising material properties for supercapacitors. J. Solid State Electrochem. **21**, 859–872 (2017)
84. Ali, A.M., Deckert-Gaudig, T., Egiza, M., Deckert, V., Yoshitake, T.: Near-and far-field Raman spectroscopic studies of nanodiamond composite films deposited by coaxial arc plasma. Appl. Phys. Lett. (2020). https://doi.org/10.1063/15142198
85. Ye, X., Zhou, H., Levchenko, I., Bazaka, K., Xu, S., Xiao, S.: Low-Temperature synthesis of graphene by icp-assisted amorphous carbon sputtering. ChemistrySelect **3**, 8779–8785 (2018)
86. Hoque, M.K., Behan, J.A., Stamatin, S.N., Zen, F., Perova, T.S., Colavita, P.E.: Capacitive storage at nitrogen doped amorphous carbon electrodes: structural and chemical effects of nitrogen incorporation. RSC Adv. **9**, 4063–4071 (2019)
87. Marchon, B., Gui, J., Grannen, K., Rauch, G.C., Ager, J.W., Silva, S., et al.: Photoluminescence and Raman spectroscopy in hydrogenated carbon films. IEEE Trans. Magn. **33**, 3148–3150 (1997). https://doi.org/10.1109/20.617873
88. Matousek, P., Towrie, M., Parker, A.: Fluorescence background suppression in Raman spectroscopy using combined Kerr gated and shifted excitation Raman difference techniques. J. Raman Spectrosc. **33**, 238–242 (2002). https://doi.org/10.1002/jrs.840
89. Casiraghi, C., Piazza, F., Ferrari, A.C., Grambole, D., Robertson, J.: Bonding in hydrogenated diamond-like carbon by Raman spectroscopy. Diam. Relat. Mater. **14**, 1098–1102 (2005). https://doi.org/10.1016/j.diamond.2004.10.030
90. Ferrari, A.C., Robertson, J.: Raman spectroscopy of amorphous, nanostructured, diamond–like carbon, and nanodiamond. Philos. Trans. R. Soc. London, Ser. A **362**, 2477–2512 (2004). https://doi.org/10.1098/rsta.2004.1452
91. Merlen, A., Buijnsters, J., Pardanaud, C.: A guide to and review of the use of multiwavelength raman spectroscopy for characterizing defective aromatic carbon solids: from graphene to amorphous carbons. Coatings (2017). https://doi.org/10.3390/coatings7100153
92. Gammage, M.D., Stauffer, S., Henkelman, G., Becker, M.F., Keto, J.W., Kovar, D.: Ethylene binding to Au/Cu alloy nanoparticles. Surf. Sci. **653**, 66–70 (2016). https://doi.org/10.1016/j.susc.2016.05.008
93. Lin-Vien, D., Colthup, N.B., Fateley, W.G., Grasselli, J.G.: The handbook of infrared and Raman characteristic frequencies of organic molecules. Elsevier, Amsterdam (1991)

94. Moskovits, M., Dilellla, D.P.: Enhanced Raman spectra of ethylene and propylene adsorbed on silver. Chem. Phys. Lett. **73**, 500–505 (1980). https://doi.org/10.1016/0009-2614(80)80704-4
95. Brolly, C., Parnell, J., Bowden, S.: Raman spectroscopy: Caution when interpreting organic carbon from oxidising environments. Planet. Space Sci. **121**, 53–59 (2016). https://doi.org/10.1016/j.pss.2015.12.008
96. Velazco, A., Béché, A., Jannis, D., Verbeeck, J.: Reducing electron beam damage through alternative STEM scanning strategies. Part I Exp. Find. Ultramicrosc. **232**, 113398 (2022). https://doi.org/10.1016/j.ultramic.2021.113398
97. Garman, E.F., Weik, M.: X-ray radiation damage to biological samples: recent progress. J. Synchrotron Radiat. **26**, 907–911 (2019). https://doi.org/10.1107/S0909049509004361
98. Leijten, Z.J., Keizer, A.D., de With, G., Friedrich, H.: Quantitative analysis of electron beam damage in organic thin films. J. Phys. Chem. C **121**, 10552–10561 (2017). https://doi.org/10.1021/acs.jpcc.7b01749
99. Worobiec, A., Darchuk, L., Brooker, A., Potgieter, H., Van Grieken, R.: Damage and molecular changes under a laser beam in SEM-EDX/MRS interface: a case study on iron-rich particles. J. Raman Spectrosc. **42**, 808–814 (2011). https://doi.org/10.1002/jrs.2789
100. Holton, J.M.: A beginner's guide to radiation damage. J. Synchrotron Radiat. **16**, 133–142 (2009). https://doi.org/10.1107/S0909049509004361
101. Lei, Y., Zhang, L., Zhou, L., Yu, J., Zhao, G., Guo, L., et al.: Proton irradiation-induced changes in the tribological performance of polyimide composites. Tribol. Int. **167**, 107427 (2022). https://doi.org/10.1016/j.triboint.2021.107427
102. Juretzka, B., Wieber, S., Wilkens, R., Hagemann, M., Kolb, R., Riedel, R.: Tribological behavior of film forming organosilane/-siloxane oil additives: film characterization and influences on lubrication. Tribol. Lett. **68**, 5 (2020). https://doi.org/10.1007/s11249-019-1241-0
103. Minfray, C., Martin, J., De Barros, M., Mogne, T.L., Kersting, R., Hagenhoff, B.: Chemistry of ZDDP tribofilm by ToF-SIMS. Tribol. Lett. **17**, 351–357 (2004)
104. Minfray, C., Martin, J., Esnouf, C., Le Mogne, T., Kersting, R., Hagenhoff, B.: A multi-technique approach of tribofilm characterisation. Thin Solid Films **447**, 272–277 (2004). https://doi.org/10.1016/S0040-6090(03)01064-2
105. Costa, H., Evangelista, K., Cousseau, T., Acero, J., Kessler, F.: Use of XANES and XPS to investigate the effects of ethanol contamination on anti-wear ZDDP tribofilms. Tribol. Int. **159**, 106997 (2021). https://doi.org/10.1016/j.triboint.2021.106997
106. Ma, H., Li, J., Chen, H., Zuo, G., Yu, Y., Ren, T., et al.: XPS and XANES characteristics of tribofilms and thermal films generated by two P-and/or S-containing additives in water-based lubricant. Tribol. Int. **42**, 940–945 (2009). https://doi.org/10.1016/j.triboint.2009.01.004
107. Heuberger, R., Rossi, A., Spencer, N.D.: XPS study of the influence of temperature on ZnDTP tribofilm composition. Tribol. Lett. **25**, 185–196 (2007). https://doi.org/10.1007/s11249-006-9166-9
108. De Barros, M.-I., Bouchet, J., Raoult, I., Le Mogne, T., Martin, J.-M., Kasrai, M., et al.: Friction reduction by metal sulfides in boundary lubrication studied by XPS and XANES analyses. Wear **254**, 863–870 (2003). https://doi.org/10.1016/S0043-1648(03)00237-0
109. Marino, M.J., Hsiao, E., Chen, Y., Eryilmaz, O.L., Erdemir, A., Kim, S.H.: Understanding run-in behavior of diamond-like carbon friction and preventing diamond-like carbon wear in humid air. Langmuir **27**, 12702–12708 (2011). https://doi.org/10.1021/la202927v
110. Tóth, A., Bertóti, I., Székely, T., Mohai, M.: XPS study of ion-induced changes on the surface of an organosilicon model polymer. Surf. Interface Anal. **7**, 282–288 (1985). https://doi.org/10.1002/sia.740070606
111. Boesenberg, U., Ryan, C.G., Kirkham, R., Jahn, A., Madsen, A., Moorhead, G., et al.: Fast XANES fluorescence imaging using a Maia detector. J. Synchrotron Radiat. **25**, 892–898 (2018). https://doi.org/10.1107/S1600577518004940
112. Holton, J.M.: XANES measurements of the rate of radiation damage to selenomethionine side chains. J. Synchrotron Radiat. **14**, 51–72 (2007). https://doi.org/10.1107/S0909049506048898
113. Azman, N.F., Samion, S.: Dispersion stability and lubrication mechanism of nanolubricants: a review. Int. J. Precis. Eng. Manuf. Green Technol. **6**, 393–414 (2019). https://doi.org/10.1007/s40684-019-00080-x
114. Kuijper, M., van Hoften, G., Janssen, B., Geurink, R., De Carlo, S., Vos, M., et al.: FEI's direct electron detector developments: Embarking on a revolution in cryo-TEM. J. Struct. Biol. **192**, 179–187 (2015). https://doi.org/10.1016/j.jsb.2015.09.014
115. Martini, A., Kim, S.H..: Activation volume in shear-driven chemical reactions. Tribol. Lett. **69**(4) (2021). https://doi.org/10.1007/s11249-021-01522-x